Direct Imaging of Exoplanets: Science & Techniques
Proceedings IAU Colloquium No. 200, 2005
C. Aime and F. Vakili, eds.

doi:10.1017/S1743921306009598

Subwavelength gratings for phase mask coronagraphy: the 4QZOG and AGPM coronagraphs

Dimitri Mawet[1] and Pierre Riaud[1]

[1]Institut d'Astrophysique et de Géophysique de Liège, University of Liège, Allée du 6 Août, 4000, Sart Tilman, Belgium
email: mawet@astro.ulg.ac.be

Abstract. We present two new phase mask coronagraphs implemented with subwavelength diffractive optical elements. The first one is an evolution of the four quadrant phase mask coronagraph (FQPM), which resolves the π phase shift chromaticity issue: the four quadrant zeroth order grating (4QZOG). The second one is a totally new design consisting of an optical vortex induced by a space-variant grating: the annular groove phase mask (AGPM) coronagraph is fully symmetric and free from any "shaded zones". The potential performances of the 4QZOG and AGPM coronagraph are very good, ensuring, for instance, a theoretical contrast of 1.4×10^{-7} at $3\lambda/D$ over the whole K band. These coronagraphs could be used alone on single-pupil telescopes either in space or on the ground (with an adaptive optics system) to detect exoplanets.

Keywords. High angular resolution, Phase mask coronagraphy, Achromatic phase shifters, Subwavelength gratings, Space-variant gratings, Optical vortices

1. Introduction

Direct detection of exoplanets around nearby stars is very difficult due to the large flux ratio between them. For example, an Earth-like exoplanet is typically 6×10^9 times fainter than its host star in the visible and 7×10^6 times fainter in the thermal infrared. Since 1996, various coronagraphs have been proposed: amplitude coronagraphs deriving from the original Lyot's design and phase-mask coronagraphs, first considered by Roddier & Roddier 1997. Amplitude coronagraphs possess a major inherent weakness: the physical extension of the opaque zone occults a significant region centered on the optical axis and thus all the sources behind it. For example, let us mention the case of the recent Notch-Filter Mask (Kuchner & Spergel 2003): this design presents a large central opaque zone extending in the focal plane up to $3\lambda/D$ (D is the telescope diameter whereas λ is the wavelength) where the potential companion is still attenuated by at least 50%. Of course this weakness reveals to be an advantage as soon as sensitivity to low order aberrations is more critical than the inner working distance. Rouan *et al.* (2000) proposed the so-called four-quadrant phase mask coronagraph (FQPM). The FQPM principle has been validated on the bench in monochromatic (Riaud *et al.* (2003)) and polychromatic light (D. Mawet *et al.*, submitted to A&A) and on the sky with a monochromatic component installed on the NAOS-CONICA instrument at the VLT (Boccaletti *et al.* (2004)). As for every phase mask, its Achilles'heels are the chromaticity issues and the presence of "dead zones", in this case on the quadrant transitions (the central obscuration is a common issue of almost every coronagraphs). Some solutions for the phase masks chromaticity issue have been presented like, for example, the dual zone phase mask coronagraph (DZPMC) which presents only a first order achromatization and must be used with a pupil apodization scheme (Soummer *et al.* (2003)). In the phase coronagraph family, let us also mention the

special cases of the achromatic interfero coronagraph (AIC) that provides achromatic π phase shift in a Michelson Interferometer (Gay & Rabbia (1996)). Finally, we must also cite pupil apodization schemes like the phase induced amplitude apodization (PIAA) where the starlight is not attenuated but redistributed (Guyon (2003)).

In this paper, we propose to remedy the two main limitations of the FQPM. First, we present the 4QZOG where the subwavelength grating technology provides a powerful and flexible solution to the chromatism issue. Secondly, we propose a new design of a phase-mask coronagraph derived from the 4QZOG that totally suppresses the annoying dead zones: the annular groove phase mask coronagraph (AGPM).

2. Subwavelength gratings

When the period Λ of the grating is smaller than the wavelength of the incident light, it does not diffract as a classical spectroscopic grating. All the incident energy is enforced to propagate only in the zeroth order, leaving incident wavefronts free from any further aberrations. The subwavelength gratings are therefore often called zeroth order gratings (ZOGs). Whether a diffraction order propagates or not is determined by the well-known grating equation from which a "ZOG condition" on the grating period to wavelength ratio can be derived:

$$\frac{\Lambda}{\lambda} \leqslant \frac{1}{n_I \sin\chi + \max\left(n_I, n_{III}\right)} \tag{2.1}$$

where χ is the angle of incidence, n_I and n_{III} are the refractive indices of the incident (superstrate) and transmitting (substrate) media, respectively. This type of gratings behaves like homogeneous media with unique characteristics, which can be used to synthesize artificial birefringent achromatic waveplates (Kikuta *et al.* (1997); Nordin & Deguzman (1999)) or monolithic anti-reflective structures (for example, Karlsson & Nikolajeff (2003)). Quarterwave or halfwave plates are extensively used in astrophysics for polarimetric studies. Subwavelength gratings constitute an elegant and flexible solution to produce them. The key point is that by carefully controlling the geometry of the grating structure (via the grating parameters: the period Λ, the depth h and the width of the grating ridges $F\Lambda$ with F the filling factor) we are able to tune the so-called form birefringence $\Delta n_{TE-TM}(\lambda) = n_{TE}(\lambda) - n_{TM}(\lambda)$ where n_{TE} and n_{TM} are the two effective indices associated with the subwavelength structure, one for each polarization state: TE (tranverse electric) and TM (tranverse magnetic). Intuitively, one can understand this artificial anisotropy and the existence of two distinct effective indices: the incident light sees two different media as its vectorial components vibrate parallel or orthogonal to the grating lines. The idea is to make the form birefringence proportional to the wavelength in order to achromatize the subsequent differential π phase shift between the two polarization states TE and TM

$$\Delta\phi_{TE-TM}(\lambda) = \frac{2\pi}{\lambda}\, h\, \Delta n_{TE-TM}(\lambda) \approx \pi \tag{2.2}$$

with h, the optical path through the birefringent medium. This is a good example of refractive index engineering. To simulate grating responses and calculate the form birefringence $\Delta n_{form} = \Delta n_{TE-TM}$ in the subwavelength and resonant domain ($\Lambda \approx \lambda$), scalar theories of diffraction dramatically fail. The vectorial nature of light must be taken into account implying a resolution of the Maxwell equations by the so-called rigorous coupled wave analysis (RCWA; Moharam & Gaylord (1981)). The RCWA gives the full vectorial diffractive characteristics of the created medium.

https://doi.org/10.1017/S1743921306009598 Published online by Cambridge University Press

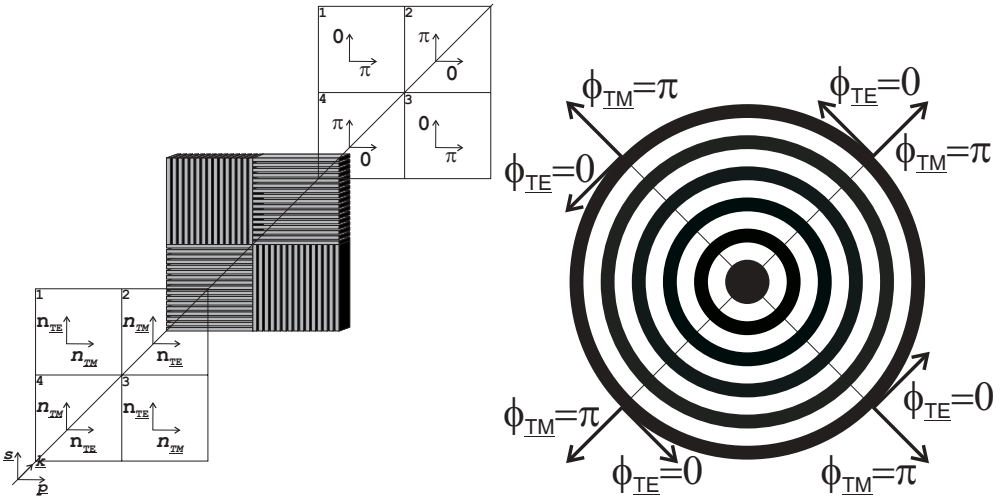

Figure 1. Left: 4QZOG implementation, where the four gratings engraved on a unique substrate are strictly identical and implemented in the following way: two of them in two quadrants along one diagonal are rotated by 90 degrees around their normals with respect to the two others. Right: AGPM implementation. The AGPM consists of a concentric circular surface-relief grating with rectangular grooves with depth h and a periodicity Λ.

3. ZOG implementation in phase-mask coronagraphy

In this section, we will first focus on the ZOG ability to induce a precise achromatic phase shift and a controlled intensity balance in order to create a destructive interference as dark as possible. Their implementation into the FQPM and after on the AGPM coronagraphs will then be discussed.

3.1. *Preliminary considerations*

The design issue consists both in the optimization of the π phase shift quality within a given spectral range for a well-chosen material and the equalization of the interfering fluxes for each polarization. The merit function to be minimized is the null depth $N(\lambda)$. The latter is directly related to the phase shift error with respect to π, $\epsilon(\lambda) = \Delta\phi_{TE-TM}(\lambda) - \pi$ and the flux ratio $q(\lambda) = \eta_{TE}(\lambda)/\eta_{TM}(\lambda)$:

$$N(\lambda) = \frac{\left(1 - \sqrt{q(\lambda)}\right)^2 + \epsilon(\lambda)^2\sqrt{q(\lambda)}}{\left(1 + \sqrt{q(\lambda)}\right)^2} \tag{3.1}$$

The ZOG technology allows to tune the form birefringence in order to minimize the phase-shift error $\epsilon(\lambda)$ but also the difference between the effective indices and the external medium indices that induces unequal TE/TM-Fresnel reflection coefficients at the interfaces. We have investigated several ways to ensure this proper flux balance, i.e. $q \approx 1$. The principle is always the same and consists in trying to minimize the index discontinuities (impedance matching) at the interfaces. The most efficient solution is to cover the ZOG with a single $\lambda/4$ layer. The latter settles at the bottom and on the top of the grating ridges. This leads to an original configuration, a 3-layer grating whose complex behavior is diffraction-governed. We demonstrate here below that this particular structure can be optimized to give very interesting results.

https://doi.org/10.1017/S1743921306009598 Published online by Cambridge University Press

3.2. *4QZOG and AGPM*

In the case of the FQPM implementation, the four gratings engraved on a unique substrate are strictly identical and implemented in the following way: two of them in two quadrants along one diagonal are rotated by 90 degrees around their normals with respect to the two others. This anti-symmetrical configuration achieves the FQPM particular focal plane π-phase distribution (Fig. 1). This new component will be referred as to the Four Quadrant-ZOG, or 4QZOG (Mawet *et al.* (2005b)). The AGPM space variant ZOG (Fig. 1) synthesizes a spiral phase plate which creates an "optical vortex". Indeed, at the center of the components, the phase possesses a screw dislocation inducing a phase singularity, i.e. an optical vortex. The central singularity forces the intensity to vanish by a total destructive interference, creating a dark core. This dark core propagates and is conserved along the optical axis. It can be demonstrated that a focal plane vortex leads to a total rejection in the ideal case (Mawet *et al.* (2005a)). Furthermore, the ZOG unique properties permit a broadband use as in the 4QZOG. Indeed, the ZOG parameters (period, depth, filling factor) are the same in the 4QZOG and AGPM configurations. As seen before, the only difference concerns the geometry of implementation which suppress the dead zones.

4. Simulation results

Presently, subwavelength gratings are more easily manufactured for the infrared domain (near and mid) because there are still technical difficulties to imprint sub-micron patterns. Fortunately, the near-term potential applications (VLT-Planet Finder, for instance) of this technology concern this wavelength domain. We will focus on the astrophysical bandfilters H ($1.475-1.825\,\mu m$), K ($2-2.4\,\mu m$) and N ($9.3-11.6\,\mu m$). We have now to chose among the restricted list of infrared materials keeping in mind that the ZOG technology is sufficiently flexible to accommodate the majority of them. We have selected diamond, zinc selenide ($ZnSe$) and silicon (Si). This choice is justified in two ways: these materials are common in infrared applications and their etching processes are well-known. Results in terms of null depth are excellent either for the H, K or N bands (Fig. 2). Indeed, the mean null depth performances are close to the 10^{-5} level over the whole spectral range of the three considered band filters. These optimal results have been calculated by implementing the simplex search method with our RCWA algorithm.

5. Expected coronagraphic performance

To assess the performance of the 4QZOG and AGPM coronagraphs, we performed numerical simulations that imply three different stages: 1- a RCWA stage where the form birefringence of the local grating is calculated; 2- an analytical treatment giving the spatial distribution of the output polarization field; 3- a scalar far-field propagation Fourier coronagraphic code with assumed wavefront qualities of $\lambda/70$ rms at 632.8 nm (current state of the art). For example, the coronagraphic profile in the K band shows a peak-to-peak null depth better than about $\approx 10^{-5}$. The speckle level of $\approx 10^{-7}$ is quickly reached at a few λ/D (see Fig. 3 for the AGPM). The AGPM coronagraphic behavior is very similar to the achromatic 4QZOG coronagraph, but with a total symmetry. As mentioned before, the FQPM/4QZOG quadrant transitions induce a non-negligible attenuation of the circumstellar features lying on them. These dead zones represent quite a significant portion of the focal plane (about 10% at $6\lambda/D$). Thanks to the perfect

https://doi.org/10.1017/S1743921306009598 Published online by Cambridge University Press

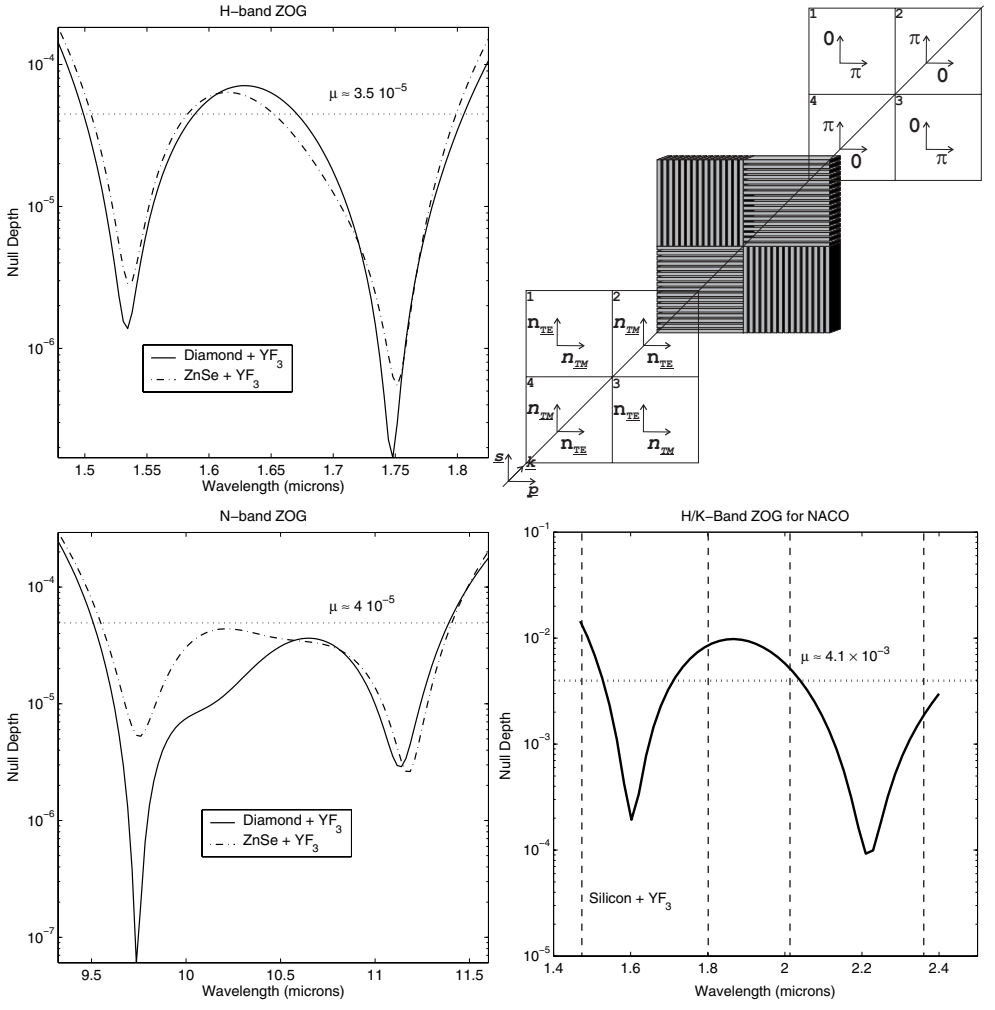

Figure 2. Top left: H-band ZOG null depth versus wavelength. The continuous curve is for the diamond YF_3 AR coated 4QZOG/AGPM. The dashed curve, for the $ZnSe\,YF_3$ AR coated one. $\mu \approx 3.5 \times 10^{-5}$ is the mean null depth over the whole H band. Top right: K-band ZOG null depth versus wavelength. $\mu \approx 1.7 \times 10^{-5}$ is the mean null depth over the whole K band. Bottom left: N-band ZOG null depth versus wavelength. $\mu \approx 4 \times 10^{-5}$ is the mean null depth over the whole N band. Bottom right: H/K-Band silicon YF_3 AR coated ZOG null depth versus wavelength. $\mu \approx 4.1 \times 10^{-3}$ is the mean null depth over both the H and K bands.

AGPM circular symmetry, this problem does not exist any more. These performances are comfortably one order of magnitude above the H-band/K-Band VLT-PF specification for example. Indeed, the main limitation for ground-based observations comes from the atmospheric turbulence residuals after adaptive optics corrections of the incoming fluctuating wavefronts. Let us emphasize that the Inner Working Angles (IWA) of the 4QZOG and AGPM are very good, peering well under λ/D. As far as stellar leakage is concerned, numerical simulations show that the AGPM null depth degrades as $\theta^2_{\lambda/D}$ close to the optical axis (Mawet *et al.* (2005a)), just as the FQPM/4QZOG (with $\theta_{\lambda/D}$, the angle from the optical axis).

https://doi.org/10.1017/S1743921306009598 Published online by Cambridge University Press

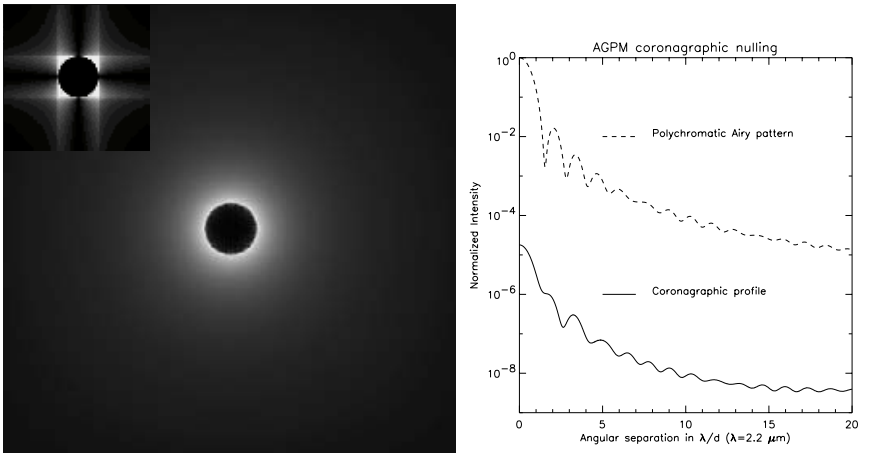

Figure 3. Left: AGPM pupil image showing the perfect annular symmetry. To be compared with the FQPM. Right: coronagraphic simulation in a realistic case with $\lambda_{vis}/70$ rms wavefronts taking into account residual chromatism and amplitude errors.

6. Conclusions

In this paper, we have presented two new phase mask coronagraphs that are inherently quasi-achromatic thanks to the subwavelength grating technology. Results in terms of global null depth are very good ($\approx 10^{-5}$). The potential performance of the 4QZOG and AGPM coronagraphs ensures, for instance, a theoretical contrast of 1.4×10^{-7} at $3\lambda/D$ over the whole K band and with an inherent perfect symmetry in the AGPM case. Thanks to the ZOG design flexibility, the 4QZOG and AGPM coronagraphs can accommodate a large variety of materials and wavelength bands thus making them an attractive solution for future instruments dedicated to high resolution/high contrast space- or ground- based imaging in the context of exoplanet detection and characterization.

Acknowledgements

D. Mawet and P. Riaud acknowledges the financial support of the Belgian "Fonds pour la formation à la Recherche dans l'Industrie et dans l'Agriculture" and the "Pôle d'Attraction Inter-Universitaire", respectively.

References

Boccaletti, A., Riaud, P., Baudoz, P., Baudrand, J., Rouan, D., Gratadour, D., Lacombe, F., & Lagrange, A.-M. 2004, *PASP* 116, 1061
Gay, J. & Rabbia, Y. 1996, *CR. Acad. Sci. Paris* 332, 265
Guyon, O. 2003, *A&A* 404, 379
Karlsson, M. & Nikolajeff, Fr. 2003, *O*pt. Express 11 (5), 502
Kikuta, H., Ohira, Y., & Iwata, K. 1997, *Applied Optics* 36, 1566
Kuchner, M.J. & Spergel, D.M. 2003, *ApJ* 594, 617
Mawet, D., Riaud, P., Absil, O., & Surdej, J. 2005a, *A*pJ in press
Mawet, D., Riaud, P., Baudrand, J., & Surdej, J. 2005b, *A*pplied Optics in press
Moharam, M.G. & Gaylord, T.K 1981, *J*OSA 71, 811
Nordin, G.P. & Deguzman, P.C. 1999, *O*pt. Express 5 (8), 163
Riaud, P., Baudrand, J., Boccaletti, A., & Rouan, D. 2003, *PASP* 115, 712
Roddier, F. & Roddier, C. 1997, *PASP* 109, 815
Rouan, D., Riaud, P., Boccaletti, A., Clénet, Y., & Labeyrie, A. 2000, *PASP* 112, 1479
Soummer, R., Dohlen, K., & Aime, C. 2003, *A&A* 403, 369

https://doi.org/10.1017/S1743921306009598 Published online by Cambridge University Press